SELF-BEARING MOTOR

– Key Technology to Implantable Artificial Heart Pump –

Yohji Okada
Dept. of Mechanical Eng., Ibaraki University, Hitachi, Ibaraki-Pref., 316-8511 Japan
okada@mech.ibaraki.ac.jp

ABSTRACT

Magnetic bearings have been used to support rotors without physical contact. However, the rotor can become long and is apt to undergo bending vibration. Several types of self-bearing motors have been proposed and developed which are combination of a rotary motor and an active magnetic bearing, thus replacing the contact components and leading to an overall size reduction. This paper introduces several types of the self-bearing motor and their characteristics. One of the most important application might be an implantable artificial heart pump. The research works of radial and axial flow blood pumps are introduced.

INTRODUCTION

Magnetic bearings can support rotors without physical contact [1],[2]. This requires a separate driving motor in addition to the magnetic bearings. As a consequence, the rotor can become long and is apt to undergo bending vibration. Several types of self-bearing motors have been introduced which are combination of a rotary motor and an active magnetic bearing [3]-[18].

The most common self-bearing motor uses two kinds of rotating magnetic flux: rotational control is achieved with the same pole number (P) of the rotor, while a pure drag force is produced by the plus two or minus two pole ($P \pm 2$) of the motor magnetic pole. The biggest problem with this type is the complicated control by using the two different rotating magnetic fluxes [3]-[6].

A simpler self-bearing motor is introduced which uses DC flux to control the radial force [7],[8]. The construction is the combination of a hybrid type active magnetic bearing (AMB) and a permanent magnet (PM) type motor.

The above self-bearing motors use reluctance force for producing the bearing force which requires relatively thin permanent magnets. Hence it has defects of low efficiency and poor reliability. Then Lorentz type self-bearing motor is developed. Both rotary torque and levitation force are produced by Lorentz principle. The permanent magnets might be thick and it has merits of good dynamic response, good linearity and high reliability [9]-[11].

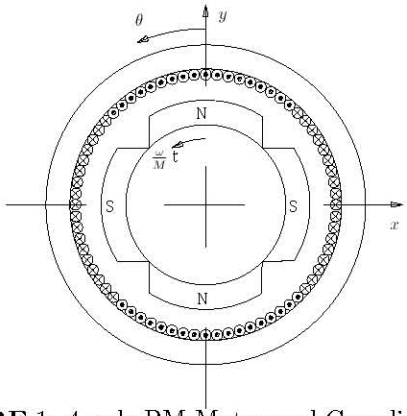

FIGURE 1: 4 pole PM Motor and Coordinate System

A simplest self-bearing motor is introduced which controls only axial displacement and gives rotary torque. The construction is similar to a bi-directional disc motor except of changing the magnitude of rotating flux to control axial attractive force [12].

In this paper the constructions and the simplified principles of the above self-bearing motors are introduced. Their experimental results and characteristics are mentioned. One of the most important application might be artificial heart pumps [13]-[17]. Radial and axial type blood pumps are introduced and discussed.

SELF-BEARING MOTORS

The principles and the experimental results of four types of self-bearing motors are introduced.

$P \pm 2$ Type Self-Bearing Motor

The most common self-bearing motor uses $P \pm 2$ theory.

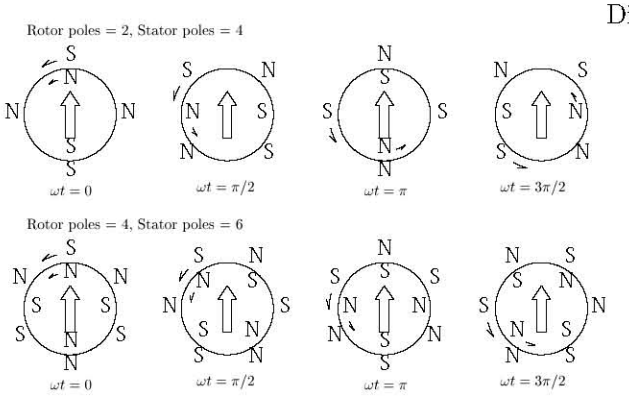

FIGURE 2: Levitation Force with +2 Pole Algorithm

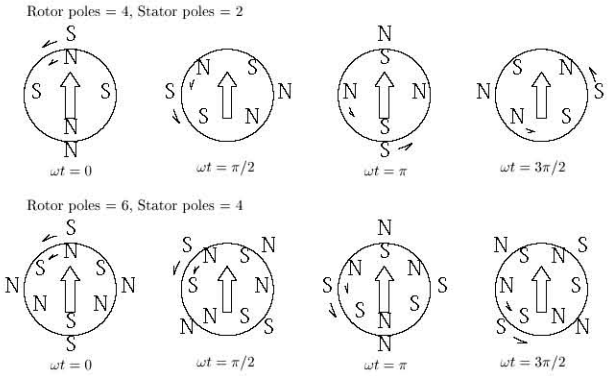

FIGURE 3: Levitation Force with −2 Pole Algorithm

Structure and Principle

Consider a rotor with M pole pair number (pole number $P = 2M$) produced by permanent magnets. The stator is assumed to have a current sheet which produces an arbitrary distributed magnetic flux. The case of $M = 2$ is shown schematically in Fig. 1.

The rotor is assumed to produce the following flux density;

$$B_r(\theta, t) = B_R \cos(\omega t - M\theta) \tag{1}$$

The stator is assumed to have the following current distribution to produce the rotating torque,

$$I_m(\theta, t) = -I_M \cos(\omega t - M\theta - \phi) \tag{2}$$

The rotating torque is controlled by changing the magnitude I_M or the angle ϕ.

In addition to the torque control current of eq. (2), a levitation control current is required. Let us consider the N pole pair current in the stator which gives the following magnetic flux,

$$B_f(\theta, t) = -B_{F1} \cos(\omega t - N\theta) - B_{F2} \sin(\omega t - N\theta) \tag{3}$$

The total levitation force in $\theta = 0$ direction is calculated by integrating the y component of attractive force [5],[6]. This calculation produces a constant force,

$$F_y = \frac{\pi B_R r L}{2\mu_0} B_{F1} \tag{4}$$

when $M - N = \pm 1$. This solution is schematically shown in Fig. 2 ($P + 2$ pole algorithm) and Fig. 3 ($P - 2$ pole algorithm).

The x-directional force is calculated by integrating the x component of the attractive force.

$$F_x = \frac{\pi B_R r L}{2\mu_0} B_{F2} \tag{5}$$

Hence, two dimensional radial position of rotor can be controlled by changing the magnitudes of B_{F1} and B_{F2}.

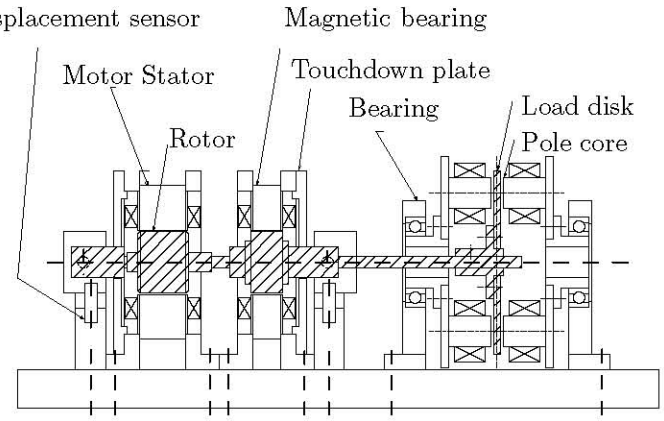

FIGURE 4: Schematic of Experimental Setup

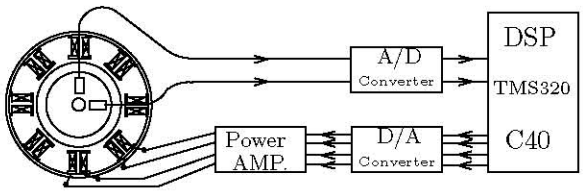

FIGURE 5: Digital Control System

Experimental Results and Considerations

To test the capability of the levitated motor, a horizontal type experimental apparatus was constructed, as shown schematically in Fig. 4. The rotor was set horizontally. The torque is added by the load apparatus, while the gravity of the rotor is the radial load to the motor. The load side of the rotor shaft is supported by a standard magnetic bearing while the free end is housed with the proposed motor. The current sheet stator is approximated by 8 concentrated wound pole stator, the current of which is controlled by the power amplifiers individually. The rotor of the motor has a diameter of 40.3 mm and a width of 35 mm, while the magnetic bearing is differ only in the width of 25 mm. The average airgap is 0.8 mm.

The levitation and rotation is controlled by a digital signal processor (DSP; $TMS320C40$). The control system is shown in Fig. 5. Four gap sensors are

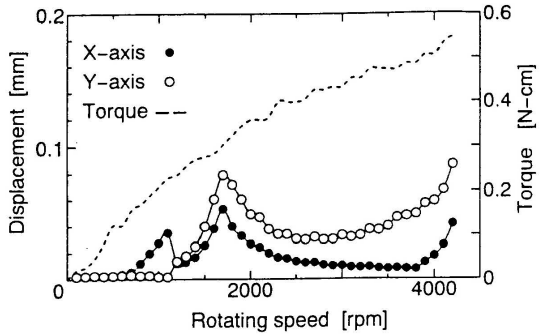

FIGURE 6: Unbalance Response and Load Torque (PM 2-pole Motor, +2 Algorithm)

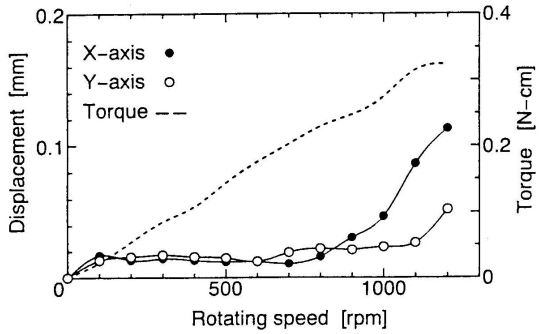

FIGURE 7: Unbalance Response and Load Torque (PM 4-pole Motor, −2 Algorithm)

installed to measure the x and y displacements of the rotor. According to the measured gap displacements, the DSP calculates each coil current from the summation of the motoring current and the levitation control current. The levitation control algorithm is the standard PD controller,

$$G(z) = K_P + \frac{K_D(z-1)}{T_D\left(z - e^{-\tau/T_D}\right)} \qquad (6)$$

where K_P, K_D and T_D are determined experimentally as $K_P = 2.0$, $K_D = 0.007$ and $T_D = 0.1$ [ms]. The sampling interval τ used is 0.1 [ms].

Two PM rotors are made and tested; 2-pole and 4-pole ones. The stator can produce two rotating magnetic fields; 2-pole and 4-pole ones. Hence two types of experiments can be performed using these two disks with the proposed $P \pm 2$ algorithm. The combined control of levitation and rotation shows promising results. The levitated unbalance responses and the load torques are shown in Figs. 6 and 7. These experiments are performed by increasing the motoring field speed stepwise by 50 [r/min]. After the rotor has reached the steady-state speed, the vibration amplitude at fundamental frequency and the load torque are recorded.

In the case of P+2 algorithm, the rotation is relatively stable. The maximum rotating speed reaches 4,200 rpm (Fig. 6).

In the case of P−2 algorithm, the rotation is

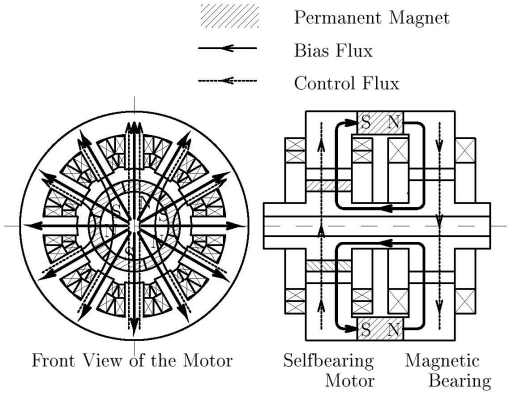

FIGURE 8: Schematic of Hybrid AMB Self-bearing Motor

weaker. The resulting unbalance response is shown in Fig. 7, which indicates relatively low maximum speed of 1,200 rpm than the previous cases of P+2 algorithm. This is mainly due to the flux distortion of the stator which in turn influence the results worsely.

Hybrid Type Self-Bearing Motor

A simpler self-bearing motor is developed which uses DC flux to control the radial force [7],[8].

Structure and Principle

The schematic drawing of the hybrid type self-bearing motor is shown in Fig. 8. The side view indicates two components; the left side is the proposed motor, while the right side is the hybrid type magnetic bearing. A bias PM is installed between them which gives the bias flux, as shown by the solid arrow lines. The radial force is produced by controlling the coil current which produces the control flux, as shown by the dotted arrow lines.

The front view indicates the construction of the proposed motor. The stator has two kinds of winding; one for levitation control and another for rotation. There are two levitation coils for the x and y directions, both of them are two pole windings. They produce the control flux, as shown by the dotted arrow lines in the figure, and produce radial forces.

Thin permanent magnets are glued on the surface of the rotor which gives a polarity of M pole pair number to the rotor. Motor coils are wound in the stator which produce the same pole pair number as the rotor. The electric angle difference between the stator current and the rotor position controls the rotating torque.

The motor coordinate system and flux distributions are shown in Fig. 9. The stator is assumed to have a current sheet which produces arbitrary distributed magnetic flux. The total flux distribution produced by PMs is indicated by the following equa-

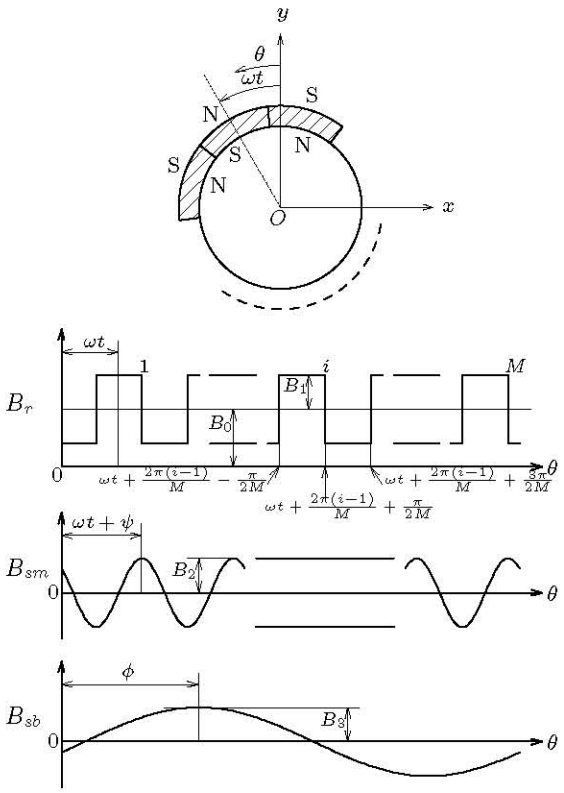

FIGURE 9: Coordinates and Flux Distributions

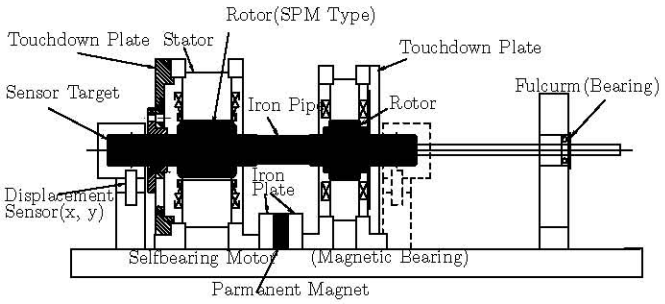

FIGURE 10: Schematic of Experimental Setup

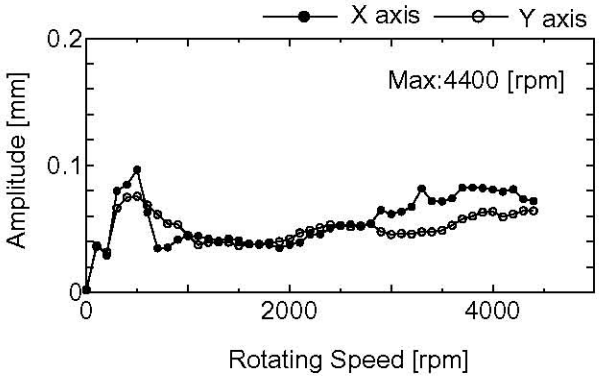

FIGURE 11: Unbalance Response when the Motoring Current is 0.5[A]

tion and is shown schematically in Fig. 9.

$$B_r = \begin{cases} B_0 + B_1 \\ \cdots \left(\omega t + \frac{2\pi(i-1)}{M} - \frac{\pi}{2M} \sim \omega t + \frac{2\pi(i-1)}{M} + \frac{\pi}{2M}\right) \\ B_0 - B_1 \\ \cdots \left(\omega t + \frac{2\pi(i-1)}{M} + \frac{\pi}{2M} \sim \omega t + \frac{2\pi(i-1)}{M} + \frac{3\pi}{2M}\right) \end{cases} \tag{7}$$

The motor coil produces the following flux distribution:

$$B_{sm} = B_2 \cos M(\theta - \omega t - \psi) \tag{8}$$

The radial force control flux B_{sb} is produced by the levitation coil current as:

$$B_{sb} = B_3 \cos(\theta - \phi) \tag{9}$$

Then the total flux distribution B_g in the air gap is given by

$$B_g = B_r + B_{sm} + B_{sb} \tag{10}$$

The radial force dF is calculated as

$$dF = \frac{1}{2\mu_0} B_g^2 rld\theta$$

Hence, the x, y directional forces F_x, F_y are calculated by integrating the x and y components of dF over the entire gap in the θ direction [7].

The minimum pole number which guarantees the control independent condition for rotation and radial force is developed as $M \geq 3$, then we have

$$F_x = \frac{B_0 B_3 lr\pi}{\mu_0} \cos\phi \tag{11}$$

$$F_y = \frac{B_0 B_3 lr\pi}{\mu_0} \sin\phi \tag{12}$$

That is, F_x and F_y are controlled by B_3 and ϕ, and is independent from the rotor angle θ and the motor control.

Also, the rotating torque T is independently controlled from the levitation control when $M \geq 2$.

$$T = -\frac{rlgMB_1 B_2 \pi}{\mu_0} \sin M\psi \tag{13}$$

That is, T is independently controlled by B_2 and ψ.

Experimental Results and Considerations

Figure 10 shows the experimental setup. The left side is the proposed selfbearing motor, while the middle is the HB type magnetic bearing. For experimental simplicity, magnetic bearing is not operated and is used as bias flux pass. The rotor is supported by a ball bearing at right end. Hence the rotor has three degrees of control freedom; two in radial coordinate and one in rotation. All three degrees can be controlled by the proposed motor.

A ferrite permanent magnet is installed on the base plate to give the bias flux. On the surface of the

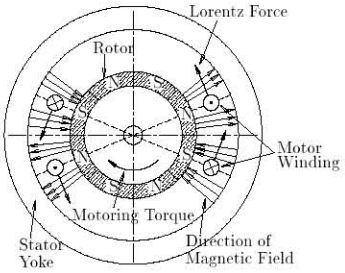

FIGURE 12: Principle of Torque Generation

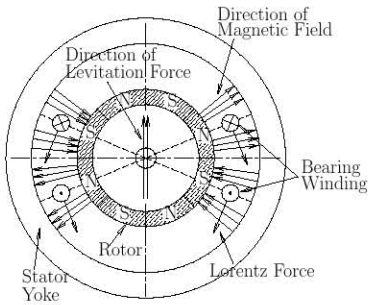

FIGURE 13: Principle of Bearing Force Generation

rotor thin permanent magnets (Neodymium magnet, thickness 0.8 mm) are glued to give the polarity to the rotor. In this paper six pole is selected. The diameter of the motor rotor is 38 mm and the length is 35 mm.

Control system is similar to the previous case. The levitation control used is the standard digital PID controller.

$$G(z) = K_P + \frac{K_D(z-1)}{T_D\left(z - e^{-\tau/T_D}\right)} + \frac{K_I \tau z}{z-1} \qquad (14)$$

The values were determined experimentally as $K_P = 25$ [A/mm], $K_D = 5$ [A sec/mm], $K_I = 0.2$ [A/sec mm] and $T_D = 30$ [ms]. The sampling interval τ is 0.1 [ms] in this case.

The stator has 12 concentrated windings, each of them are controlled individually by a digital signal processor (DSP; $TMS320C40$). Two gap sensors were used to measure the x and y displacements of the rotor. According to the measured gap displacement, the DSP calculates each coil current from the summation of the motoring current and the levitation control current. Then they are fed to each power amplifier through D/A converter.

The unbalance response is tested and the results are shown in Fig. 11. The rotor can run up to 4,400 [rpm]. By grasping the shaft, strong rotating torque was felt. However, the top speed is limited due to the higher harmonics of the flux distribution produced by the surface permanent magnets.

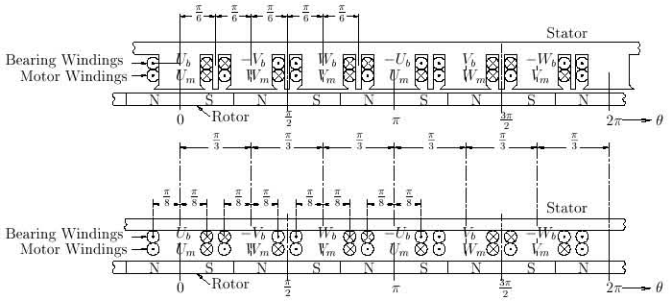

FIGURE 14: Arrangement of Motor and Bearing Windings

Lorentz Type Self-Bearing Motor

Lorentz type self-bearing motor is proposed which uses Lorentz force to produce motor torque and bearing forces [9]-[11].

Structure and Principle

Figure 12 depicts the cross section of the cylindrical motor with eight strong permanent magnets mounted on the rotor and twelve coil windings, six for motoring and six for levitation. Now, consider a pair of facing motor coils. The Lorentz forces exerted on the stator coils are aligned along the counterclockwise direction for the given current flow directions. The reaction torque for motoring the rotor is then produced in the clockwise direction.

The levitation coils are wound at the same circumferential location, the current flow direction of the right side is reversed, resulting in the Lorentz force vectors as shown in Fig. 13. The resultant force becomes a pure radial force. Six equi-angular spaced levitation coils can generate a radial force at any position.

The expanded schematics with the slotted and the slotless stators are shown in Fig. 14. These figures show the radial motors unwrapped along their circumference. The entry and return paths of each coil windings are set to be $\frac{\pi}{4}$ apart. The U, V and W coils are placed $\frac{\pi}{3}$ apart.

Suppose that the air gap flux produced by the rotor PMs can be well approximated as

$$B_g = -B\sin(\omega t + 4\theta) \qquad (15)$$

The motoring coils are driven by the three phase currents, i.e.

$$\begin{aligned} I_{U_m} &= A\cos(\omega t + \psi) \\ I_{V_m} &= A\cos(\omega t + \frac{2}{3}\pi + \psi) \\ I_{W_m} &= A\cos(\omega t + \frac{4}{3}\pi + \psi) \end{aligned} \qquad (16)$$

From Eq. (16), the current distribution along the semi-circular stator part from $-\frac{\pi}{8}$ to $\frac{7\pi}{8}$ is written

as

$$\begin{aligned} i_m &= I_{U_m}\left[\delta(\theta+\frac{\pi}{8})-\delta(\theta-\frac{\pi}{8})\right] \\ &+ I_{W_m}\left[\delta(\theta-\frac{5}{24}\pi)-\delta(\theta-\frac{11}{24}\pi)\right] \\ &+ I_{V_m}\left[\delta(\theta-\frac{13}{24}\pi)-\delta(\theta-\frac{19}{24}\pi)\right] \end{aligned} \quad (17)$$

The torque produced can then be calculated as [9].

$$T = 2rl\int_{-\frac{\pi}{8}}^{\frac{7}{8}\pi} B_g i_m d\theta = 6rlAB\cos\psi \quad (18)$$

Note that the torque, independent of the rotor position and the time, can be controlled by the motoring current magnitude A and phase ψ.

The levitation coils are driven by the three phase currents, i.e.

$$\begin{aligned} I_{U_b} &= C\cos(\omega t+\phi) \\ I_{V_b} &= C\cos(\omega t+\frac{2}{3}\pi+\phi) \\ I_{W_b} &= C\cos(\omega t+\frac{4}{3}\pi+\phi) \end{aligned} \quad (19)$$

From Eq. (19) and the current distribution expressed similar to Eq. (17), the levitation force can be calculated as [9]

[y directional force]

$$F_y = l\int_{-\frac{1}{8}\pi}^{\frac{15}{8}\pi} B_g i_b\cos\theta d\theta = \frac{3\sqrt{2+\sqrt{2}}}{2}BlC\cos\phi \quad (20)$$

[x directional force]

$$F_x = l\int_{-\frac{1}{8}\pi}^{\frac{15}{8}\pi} B_g i_b\sin\theta d\theta = -\frac{3\sqrt{2+\sqrt{2}}}{2}BlC\sin\phi \quad (21)$$

Equations (20) and (21) indicate that levitation of the rotor is achieved solely by the levitation coil control, independent of the rotation control. Note that the levitation force can be controlled by the levitation current magnitude C and phase angle ϕ.

Experimental Results and Considerations

Experiments were carried out in order to verify the theoretical development. The schematic of the experimental setup is shown in Figure 15. The cylindrical inner rotor is vertically hung by a ball bearing, allowing the planar motion of the rotor in the x and y directions.

Rotating the levitated motor and recording the steady state vibration measured the unbalance responses. The results are shown in Fig. 16.

The highest vibration of slotless type is recorded at 2400 [rpm], which is considered to be the influence

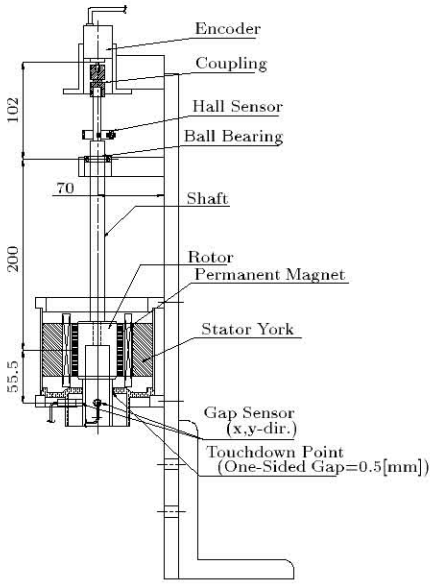

FIGURE 15: Schematic of Experimental Setup

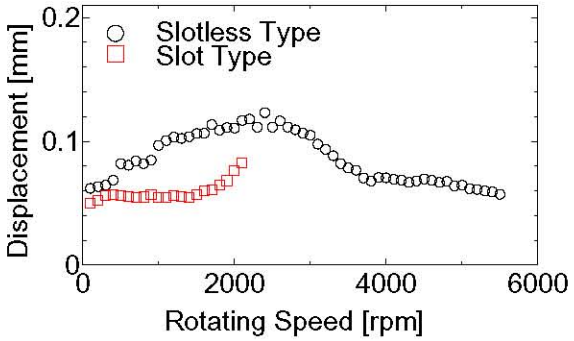

FIGURE 16: Unbalance Response

of the rigid mode. The top speed is restricted to 5500 [rpm] to avoid the centrifugal tear off of the permanent magnets, and can thus be improved by redesign.

The slot type motor can run up to 2100 [rpm]. Near this top speed however, the levitation voltage approaches the supply voltage and the levitation becomes unstable. This is considered to be the result of the high inductance of the slotted coil leading to high Back-Electromotive-Voltage.

Axial Self-Bearing Motor

Axial type self-bearing motor has the merit of simple construction and control mechanisms [12].

Structure and Principle

Figure 17 shows the schematic structure. It consists of two opposite stators and a rotor, which is similar to a bi-directional disc motor. But the magnitude of driving current for each stator is controlled according to the rotor position. The radial direction

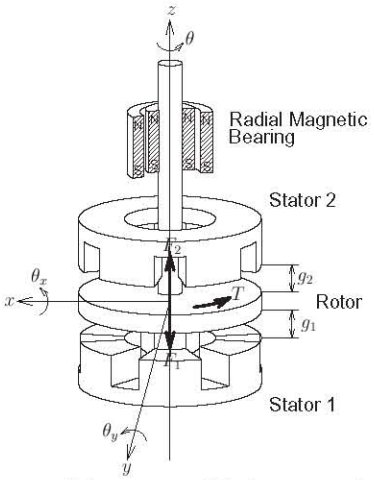

FIGURE 17: Schematic of Bidirectional Axial Self-Bearing Motor

should be stabilized by other methods (PM repulsion magnetic bearing in this case). On the upper and lower surfaces of the rotor, there are four PMs that are two N poles and two S poles by turns. While each stator has six cores with three-phase windings. The fluxes from the stator windings and the PMs produce the magnetic attractive force as well as motor torque.

Assuming that the magnetic flux density generated by PMs of the rotor is sinusoidal,

$$B_r(\theta, t) = B_R \cos(\omega t - 2\theta) \quad (22)$$

Similarly, the magnetic flux density generated by the stator windings is written as

$$B_s(\theta, t) = B_S \cos(\omega t - 2\theta - \psi) \quad (23)$$

Then, the single stator case leads to the simple expressions of the axial force F and the motoring torque T as [12]

$$F = \frac{A_r}{4\mu_0}(B_R^2 + 2B_R B_S \cos\psi + B_S^2) \quad (24)$$

$$T = \frac{A_r g_0}{2\mu_0} B_R B_S \sin\psi \quad (25)$$

Now, let us expand the axial force of Eq. (24) and the motoring torque of Eq. (25) to the bi-directional case. The peak value B_S of Eq. (23) can be written about the upper and lower stators as

$$B_{S_{upper}} = B_M + B_C \quad (26)$$

$$B_{S_{lower}} = B_M - B_C \quad (27)$$

From the equations (24) and (25), we have,

$$F_{total} = \frac{A_r}{\mu_0}(B_R \cos\psi + B_M)B_C \quad (28)$$

$$T_{total} = \frac{A_r}{\mu_0} B_R B_M \sin\psi \quad (29)$$

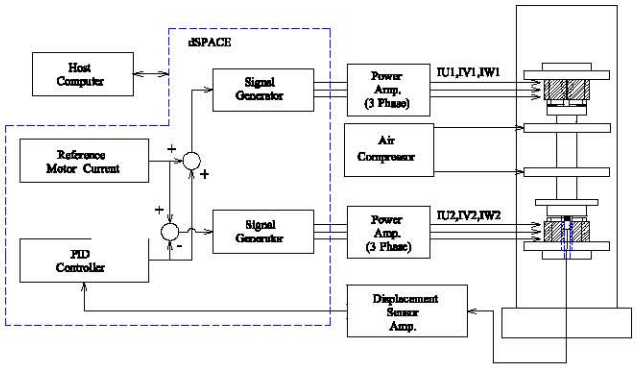

FIGURE 18: Control System

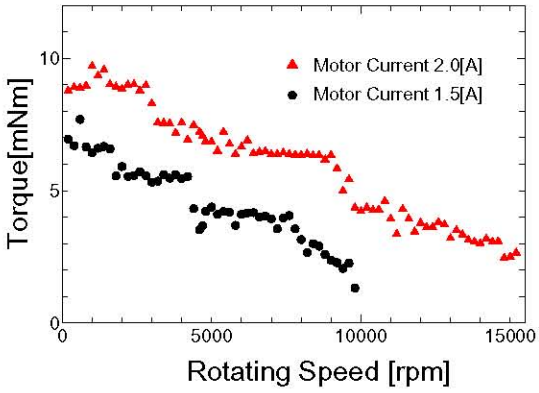

FIGURE 19: Dynamic Torque

Note that in this case, one can control the axial motion of the rotor, not affecting the motoring torque.

Experimental Results and Considerations

To confirm the capability of the proposed theory, experimental apparatus was constructed and tested. The control system is shown in Fig. 18. For levitation, the axial displacement of the rotor measured by a proximity probe is transformed into a DSP (dSPACE DS1103) and the calculated controller output is added to or subtracted from the amplitude of motor current. Then, two sets of three-phase currents are generated and fed to the stators through a six-channel power amplifier. The levitation control uses a standard PD controller.

The dynamic torque was also measured for the single stator and rotor as shown in Fig. 19. The torque is maximum at non-rotational condition and decreases according to the rotational speed.

The levitated rotating test was carried out for the bi-directional self-bearing motor in air. The unbalance response is shown in Fig. 20. Here, one can see that the levitation is very stable up to the top speed of 6,000 rpm. In this case, an air bearing was used to improve the lateral stability.

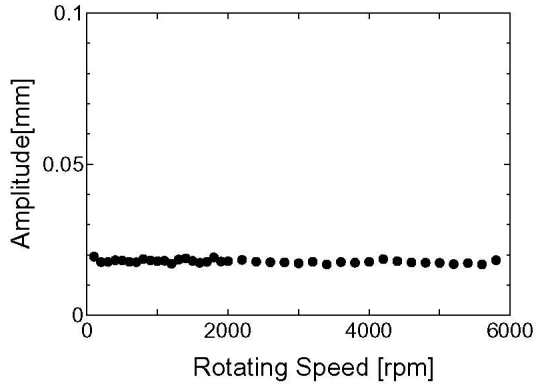

FIGURE 20: Maximum Amplitude of Axial Displacement

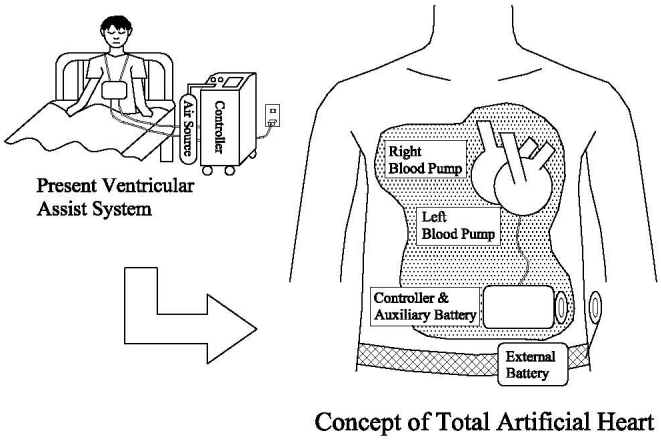

FIGURE 21: Concept of Implantable Artificial Heart

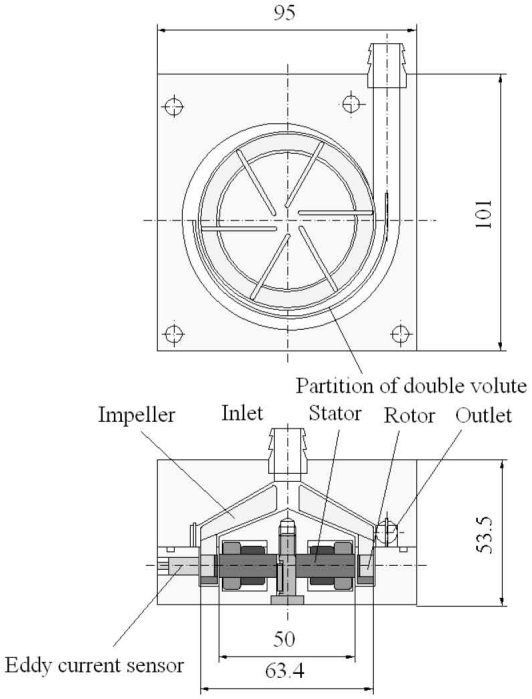

FIGURE 22: Centrifugal Blood Pump

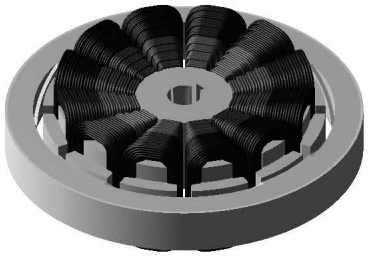

FIGURE 23: Outer Rotor Self-Bearing Motor

ARTIFICIAL HEART PUMP

The most important application of self-bearing motor is the implantable artificial heart pump.

Motivation

Heart transplant has started in Japan, 1998. Due to the religious reason translpant is still low number. Japanese legal death is the heart death which also restricts heart transplantation. Implantable artificial heart is highly requested. Figure 21 indicates the schematical concept of this project. Now the artificial blood pump is available in the hospital. If implantable heart pump has been developed the heart patient can come back to the social activities. Rotary blood pump is small and adequate for this purpose. A miniature magnetically levitated rotor is highly requested.

Centrifugal Pump with Radial Motor

Figure 22 shows the magnetically levitated centrifugal pump with outer rotor type self-bearing motor [13]-[15]. An impeller of the centrifugal pump with six open type vanes was set on the rotor. The centrifugal pump has a double volute in order to minimize the fluid dynamic imbalance inside the centrifugal pump.

Figure 23 shows the radially suspended self-bearing motor. The outer rotor structure, that a rotor is set around a stator, is adopted to miniaturize the self-bearing motor. The rotor, which is a yoke itself, has four thin permanent magnets on inner circumferential surface. The thickness of the permanent magnets is 0.7 mm. The outer diameter, the inner diameter and the thickness of the rotor are 63.4 mm, 53.4 mm, and 8 mm, respectively. The stator has twelve radial poles. The pole has a bulge at the end faced on the rotor to distribute the magnetic field effectively and a narrow radial spoke to wind coil wire. The diameter and the thickness of the prototype stator are 50 mm, 8 mm, respectively. Rotation coils to produce 3-phase 4-pole magnetic field and levitation coils to produce 2-phase 6-pole magnetic field are

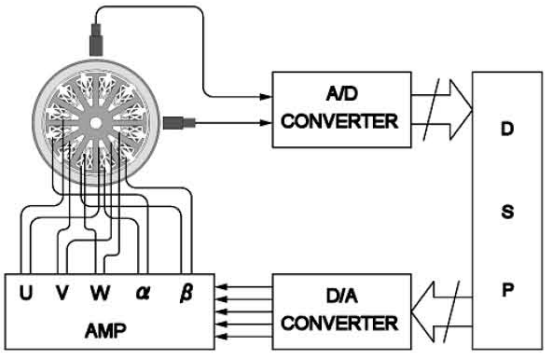

FIGURE 24: Control System of Self-Bearing Motor

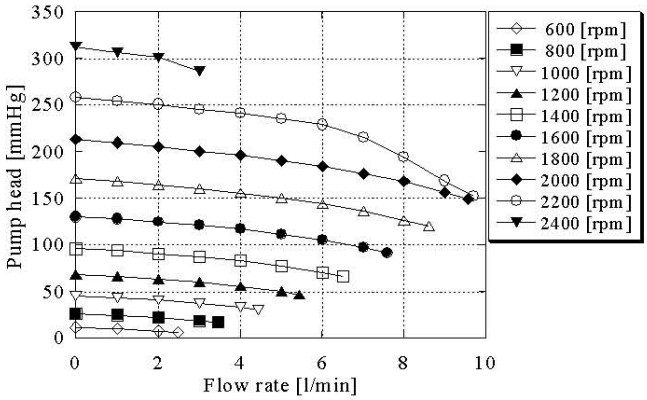

FIGURE 25: Head and Flow Rate of Centrifugal Pump

constructed separately in the stator. The $P \pm 2$ algorithm is adopted to levitate and rotate the rotor. Radial gap between the rotor and the stator is set as 1 mm. Closed magnetic circuit was formed through the stator pole and the rotor yoke.

Figure 24 shows the schematics of control system. Levitation and rotation of the rotor were controlled by a DSP. Two eddy current sensors are used to measure rotor radial position.

The pump performance, the total power consumption of the maglev pump are shown in Figure 25 and Figure 26, respectively. The levitated rotor could be rotated up to a rotational speed of 2400 rpm with pumping. The maximum flow rate and the maximum head pressure were 9.7 l/min and 313 mmHg, respectively. The maximum total efficiency was 11 %. The input electric power and pump efficiency with a pressure head of 100 mmHg and a flow rate of 5 l/min were 12 W and 9 %.

This system has been improved and the hemolysis test has been started. The results may be reported in the near future.

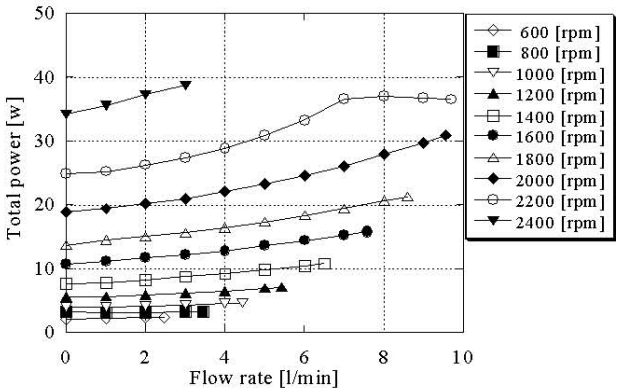

FIGURE 26: Total Power Consumption

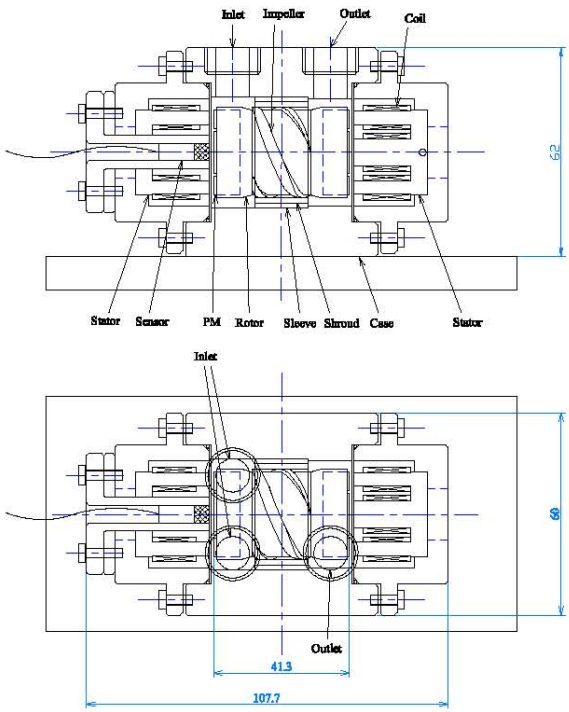

FIGURE 27: Schematic of Axial Flow Pump

Axial Flow Pump with Axial Motor

Axial flow blood pomp has the merit of small size and easy implantation. However, it requires high rotating speed and compact size for the driving motor [16],[17]. For this purpose the axial self-bearing motor mentioned before (the system in Fig. 18) is adopted.

An axial flow pump equipped with the axial self-bearing motor was designed and fabricated, which is schematically shown in Fig. 27. In this pump, a hydrodynamic blood bearing was used in the middle of the pump. The rotor with impeller could successfully levitate and rotate. Figure 28 shows the measured pump head and flow rate characteristics. The pump test recorded the maximum head of 50 mmHg and the maximum flow rate of 2.8 l/min at the rotating

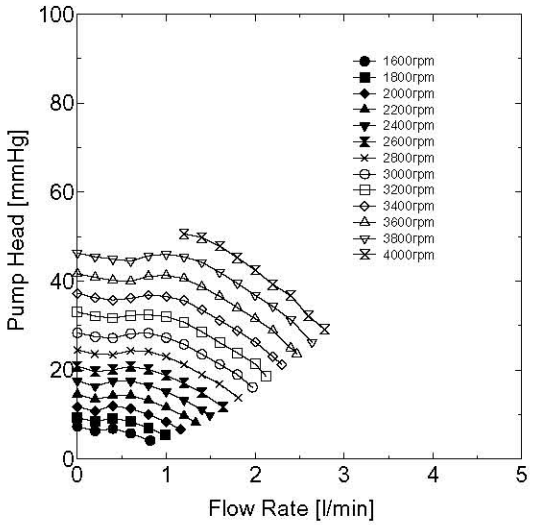

FIGURE 28: Flow Rate and Head of Axial Pump

speed of 4,000 rpm. However this performance is not enough for the practical use. It seems to be due to the non-optimum design of the pump and the insufficient motor torque considering the brake torque of hydrodynamic bearing.

The system is changed to use the double mixed flow pump. The design and the experimental resuts are reported in this symposium. Further modification is planned to miniaturize the system with full magnetic suspension.

CONCLUDING REMARKS

Four types of self-bearing motors are introduced and their test results are shown. The data reported here are from the old experiments. The systems have already been improved. A new type of self-bearing motors are also reported, ex. [18]. The implantable artificial heart pump is one of the most important application. Centrifugal and axial flow pumps are reported which are under development.

References

1. Y. Okada, et. al., JSME Publication on New Technology Series, No. 1, Magnetic Bearings - Fundamental Characteristics, Design and Applications, Yokendo Ltd., Tokyo, 1995, in Japanese (translated into Korean)
2. Schweitzer, G., et al., "Active Magnetic Bearings", Hochschulverlag AG an der ETH Zurich, 1994
3. Bichsel, J., "The Bearingless Electric Machines," *NASA Conf. on Magnetic Suspension Technology*, 1992, pp. 563-570
4. Chiba, A., et. al., "Radial Force in a Bearingless Reluctance Motor," *IEEE Trans. Magnetics*, 27(2), 1991, pp. 786-791
5. Okada, Y., et al., "Levitation Control of Permanent Magnet (PM) Type Rotating Motor", *Proc. of Magnetic Bearings, Magnetic Drives and Dry Gas Seals Conf. Exhibitions*, Alexandria, VA, USA, 1992, pp. 157-165
6. Okada, Y., et. al., "Analysis and Comparison of PM Synchronous Motor and Induction Motor Type Magnetic Bearings", *IEEE Trans. on Industry Applications*, 31(5), 1995, pp. 1047-1052
7. Okada, Y., et. al., "Hybrid AMB type Selfbearing Motor", *Proc. of 6th Int. Symp. on Magnetic Bearings*, MIT, Cambridge, 1998, pp. 497-506
8. Kanebako, H, and Okada, Y., "New Design of Hybrid-Type Self-Bearing Motor for Small, High Speed Spindle", *IEEE/ASME Trans. on Mechatronics*, Vol. 8, No. 1 March 2003.
9. Okada, Y., et. al., "Lorentz Force type Self-Bearing Motor", *Proc. of 7th Int. Symp. on Magnetic Bearings*, ETH Zurich, 2000, pp. 353-358

   vspace-2mm

10. Stephens, L. S., and Kim, D.-G., "Force and Torque Characteristics for a Slotless Lorentz Self-Bearing Servomotor", *IEEE Trans. on Magnetics*, Vol. 38, No. 4, 2002, pp. 1764-1773
11. Han, W.-S., Lee, C.-W., and Okada, Y., "Design and Control of a Disk-Type Integrated Motor-Bearing System", *IEEE/ASME Trans. on Mechatronics*, Vol. 7, No. 1, March 2002, pp. 15-22
12. Ueno, S., and Okada, Y., "Characteristics and Control of a Bidirectional Axial Gap Combined Motor-Bearing", *IEEE/ASME Trans. on Mechatronics*, Vol. 5, No. 3, September 2000, pp. 310-318
13. Masuzawa, T., et. al., "Magnetically Suspended Rotary Blood Pump with Radail Type Combined Motor-Bearing", *Artificial Organs*, Vol. 24, 2000, pp. 469-474
14. Masuzawa, T., et. al., "Magnetically Suspended Centrifugal Blood Pump with an Axially Levitated Motor", *Artificial Organs*, Vol. 27, 2003, pp. 631-638
15. Onuma, H., et. al., "Magnetically Levitated Centrifugal Blood Pump with Radially Suspended Self-Bearing Motor", *Proc. of 8th Int. Symp. on Magnetic Bearings*, Mito, Japan, August 26-28, 2002, pp. 3-8
16. Ohmori, K., et. al., "Design of an Axial-Type Self-Bearing Motor for Small Axial Pump", *Proc. of 8th Int. Symp. on Magnetic Bearings*, Mito, Japan, August 26-28, 2002, pp. 21-26
17. Okada, Y., et. al., "Axial Type Self-Bearing Motor for Axial Flow Blood Pump", *Artificial Organs*, Vol. 27, 2003, pp. 887-891
18. T. Takemoto, et. al., "A Principle and a Design of a Consequent-Pole Bearingless Motor", *Proc. of 8th Int. Symp. on Magnetic Bearings*, Mito, Japan, August 26-28, 2002, pp. 259-264